Polymer 283 (2023) 126148

Contents lists available at ScienceDirect

Polymer

journal homepage: www.elsevier.com/locate/polymer

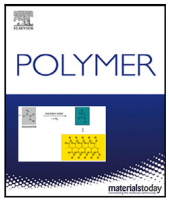

# Length-scale discrepancy in the properties of epoxy resin specimens

P. Laurikainen *, S. Bhusare, G. Mohanty, E. Sarlin

*Tampere University, Faculty of Engineering and Natural Sciences, PO Box 589, FI-33014, Finland*

ARTICLE INFO

*Keywords:*
Epoxy resin
Nanoindentation
Molecular Dynamics
Curing characteristics

ABSTRACT

In studies of the fibre-matrix interphase with microscale single fibre methods, the dependence of results on conversion of the thermoset resin – or degree of cure as it is often called – remains an issue. In the microbond method specifically, the curing of picolitre volume drop-on-fibre systems differs significantly from that of macroscale resin batches. The surface-to-volume ratio and vapour pressure can cause volatile components of the resin to evaporate, potentially limiting the degree of cure. Atomistic scale modelling along with experimental thermal analysis were used to understand the curing process and how it translates to resin properties, while nanoindentation was used to experimentally compare the mechanical performance of samples prepared in different length-scales. The evaporation is experimentally verified. Comparable variation in mechanical properties is shown in atomistic scale models of the epoxy network with no evaporation. The origin is in the network morphologies created by varying the curing process. Thus attributing the length-scale discrepancy solely to conversion is likely an oversimplification and understanding the network morphology from different curing conditions is also needed.

## 1. Introduction

While microscale testing methods are quite widely used for characterising the composite interphase, the discussion surrounding different approaches and the analysis of the results has been conflicted. Several reliable concepts for testing systems have been proposed [1–4], each with their own strengths and drawbacks. Many of the latter relate to the time, effort and reliability of preparing the prerequisite microcomposite samples. The scientific discussion, however, tends to revolve around the theory and physical relevance of the measured results, spanning from the reliability of the analytical methods to problems related to the performance, and length-scale related differences of the samples compared to macroscopic composite laminates and structures.

For the microbond test [1,3], the biggest problems are related to the drop-on-fibre sample preparation, more precisely to the curing of the thermoset resin droplets [5,6]. Generally the embedded length of these droplets ranges from tens to hundreds of micrometers. In such samples, the total volume of the resin is in the range of picolitres, while the surface area ranges in thousands of square micrometers. Thus, it can be expected for the curing process to be hindered by various surface related physico-chemical phenomena — many of which correlate with the surface-to-volume ratio. Significant surface-to-volume ratios are rarely present in macroscale resin or composite samples making these phenomena in most cases insignificant at larger length-scales. Similar problems are also encountered with the oxidisation and crystallisation of thermoplastic resin droplets, but are outside the current scope for this study.

Zinck et al. [7] have shown that epoxy matrix in microcomposite samples differs from bulk and that, due to the more ductile behaviour of the resin, plastic deformation plays a significant role in microbond testing. Similarly, Rahmani et al. [8] showed that altering the cure cycle affects the results of the microbond test results, especially if the degree of cure is below a specific threshold (approx. 80% achievable maximum for the resin used in the study). Both of these studies largely ignore the massive length-scale difference between bulk scale samples used to study resin properties and the microdroplets they supposedly represent. Zinck et al. [7] acknowledged the possibility of volatile evaporation as a complication for microdroplet curing. Rao and Drzal [5] studied the glass transition temperature of microcomposite samples and noted significant differences with resins that also correlate with the molecular weight, and thus volatility, of the resin components. Evaporation of small molecular weight components from the reactive mixture can limit the achievable degree of cure either through uneven stoichiometry for epoxies [5,9–12], or (localised) depletion of styrene from polyester and vinyl ester resins.

Thomason [13] recently reviewed many of the length-scale related problems in microdroplet preparation and highlighted the vapour pressure of the various resin components, which can include various small molecular weight organic molecules such as amines, styrene, epoxides,

* Corresponding author.
*E-mail address:* pekka.laurikainen@tuni.fi (P. Laurikainen).

https://doi.org/10.1016/j.polymer.2023.126148
Received 1 February 2023; Received in revised form 20 June 2023; Accepted 25 June 2023
Available online 24 July 2023

anhydrides and alcohols. Moisture content of the droplet was also pointed out as a potential problematic parameter of the curing process and microdroplet properties [13]. His overview concluded that after a suitably high degree of cure – if achieved – the effect of the degree of cure on the microbond test results becomes almost negligible. This conclusion is also supported by finite element (FE) simulations of the role of resin mechanical properties in the test [14].

Other studies on thermoset epoxy resins have highlighted the possible formation of different nanoscale morphology or nanostrucutres in the resin [9,11,15–18]. The core concept being that under specific conditions – or when using certain chemical components in the resin mixture – the epoxy can form regions of high crosslink density connected with regions of significantly less of crosslinks. This would result in materials, with very different properties despite a similar average conversion, and which exhibit varying contributions of solid-like and liquid-like properties [17]. Experimental evidence of length-scale related discrepancy in mechanical performance has also been noted outside the expected probability of encountering defects as damage initiation sites [19].

More general studies on epoxy curing tend to focus either on computational methods [20,21] or experimental methods, such as differential scanning calorimetry (DSC) [22,23] and rheometry [24]. These established approaches suffer from significant gaps in length-scale evoking a question how to attempt a comprehensive approach by combining the methods. The curing process is a complex physico-chemical process involving reaction energetics, molecular mobility, network morphology and surface related effects such as the aforementioned evaporation. Currently no computational method can cover all of these, especially in a single simulation, mainly due to the very different length-scale – and the accompanying system size dependent computational cost – associated with each phenomenon. Conversely, a majority of experimental methods, whether aimed for reaction energetics or physical properties utilise samples with dimensions in the millimetre scale or higher. Bridging these gaps, i.e. figuring out the connections between molecular simulations and experimental methods, is a massive ongoing challenge in the field. Unger et al. [12] compared iterative Molecular Dynamics (MD) crosslinking simulations with near-IR spectroscopy based monitoring of the curing process and found the model to fit experimental data reasonably well. For amine-cured epoxies, a more representative crosslinking simulation can be achieved by determining the relative reaction rates for the primary and secondary reactions to be used as and additional parameter for selection of crosslinking sites [21]. The implementation of a reactive force-field [25] or reactive model [26] can improve the simulations further. Recent efforts to parametrise and utilise such force-fields for crosslinked polymer systems are showing promising results for both bond formation and bond dissociation [27–29] but at a high computational cost.

Nanoindentation has proved a powerful tool for studying the mechanical properties of crosslinked polymer samples that are otherwise difficult to measure, such as thin films [30,31]. Ligot et al. [31] discuss in detail the effects the conversion and sample characteristics have on the results. Hardness, modulus, their ratio and the viscoelastic and creep behaviours are all shown to change with crosslinking as expected. Thin samples on a substrate can show effects from the substrate if the indentation depth is too deep and conversely various sample surface related effects are discussed, at least briefly. Of special interest are results with lower crosslinking degree exhibiting higher stiffness, which were attributed to molecular mobility and/or atmospheric surface effects [31].

In this study, the conversion of unreacted epoxy and amine to the crosslinked epoxy network was explored with atomistic scale simulations for a simple commercial epoxy resin system to estimate the role of conversion to the measurable material properties such as elastic modulus. The simulation outputs were compared to experimental results from macroscale samples with dimensions in the range of several millimetres, and from microscale drop-on-fibre samples with a high surface-to-volume ratio. Nanoindentation was used as the primary method for experimental characterisation of the resin mechanical properties. Thermal analysis methods, such as differential scanning calorimetry (DSC) and Fourier transform infrared spectroscopy coupled thermogravimetric analysis (TGA-FTIR) were used to empirically study the curing process and any related evaporation of volatiles. These samples were considered as representative of the macroscale behaviour only. This combined methodology was intended to explore the role of conversion – degree of cure – to the microdroplet sample behaviour and further elucidate some of the issues faced when preparing such samples. The hypothesis that the evaporation is not the only reason for the length-scale discrepancy was explored by mitigating its role whenever possible outside the TGA-FTIR measurements specifically intended for studying it.

## 2. Experimental

### 2.1. Materials

The resin system used for the experiments was EPON 828 cured with Jeffamine D–230 provided by Huntsman. The EPON 828 resin is a diglycidyl ether of bisphenol–A (DGEBA) epoxy resin with an epoxy equivalent weight of around 190 g/mol [32]. Jeffamine D–230 is poly(oxypropylene) diamine hardener with an average repeating unit count of approximately 2.5 and an amine hydrogen equivalent weight of 60 g/mol [33] subsequently denoted as polyetheramine (PEA). The schematic structures of the molecules are presented in Fig. 1. The stoichiometric mixing ratio is 100:32 by weight. All resin batches were mixed with high shear speeds until visually determined as homogeneous, the actual mixing time depended on batch volume. After mixing the batch was placed in vacuum for 3 min for gas removal.

Macroscopic samples were prepared by casting the resin in open top moulds and cured accordingly to their respective curing cycles denoted in the sample name: Bulk RT cured for 24 h at room temperature, Bulk 50 for 8 h at 50 °C, Bulk 80 (and Bulk ref) for 8 h at 80 °C and the Bulk RT-50 and Bulk RT-80 combinations of the previous. Microdroplet specimens were prepared as in previous studies featuring the microbond method [3,14,34] resulting in drop-on-fibre samples with embedded lengths ranging between 60 and 200 μm and cured for 8 h at 80 °C. While waiting for indentation the samples were kept in a controlled environment at room temperature in sample storage cabinet intended for storing electron microscopy samples.

### 2.2. Experimental methods

Thermogravimetric analysis (TGA) utilised a Netzsch TG 209F3 *Tarsus* (NETZSCH-Gerätebau GmbH, Germany) coupled to a Bruker Tensor 27 FTIR (Bruker, Germany). TGA measurements were conducted for an unreacted resin mixture and the components of the resin mixture separately. A coupling to the FTIR was included to analyse any evaporating species for their chemical composition. This coupled analysis was used to identify whether the PEA, DGEBA or a combination of the two is primarily evaporated from the resin mixture during the cure cycle. A dynamic heating step was used in the test from −20 to 350 °C with a heating rate of 10 K/min.

Differential scanning calorimetry (DSC) was used to analyse the degree of cure of the bulk resin samples. Dynamic heating from −20 °C to 300 °C was used to determine the glass transition temperature ($T_g$) from the initial curing and to determine the residual curing enthalpy. The samples were then cooled to −20 °C followed by another dynamic heating step from −20 to 300 °C to ensure no residual reactive potential and that the glass transition matches the fully cured state. Total curing enthalpy was determined by using the same heating steps for an uncured resin mixture. Comparing the residual enthalpy to the total enthalpy of the uncured systems enables the determination of degree of cure relative to the practical maximum, which is rarely equal to

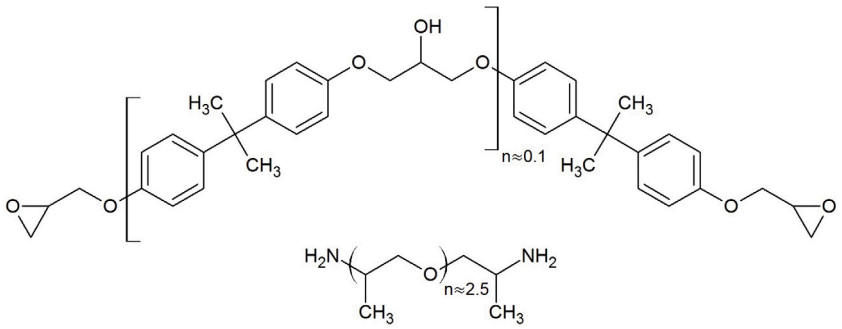


**Fig. 1.** DGEBA and PEA comprising the epoxy system used in this study. The repeating unit numbers are representative of the used grades.

the theoretical maximum determined by the stoichiometric amount of functional groups due to very restricted molecular mobility at the later stages of cure [24].

Nanointendation tests were carried out with an Alemnis in-situ nanoindenter (Alemnis AG, Switzerland) integrated inside a Scanning Electron Microscope (SEM, Zeiss LEO 1450, Germany). A cube corner pyramidal tip was used for all the indentations performed in this study. Cube corner tip has a smaller included angle and hence, provides better viewing angle for tip positioning on the microdroplet samples compared to the widely used Berkovich tip.

The indents comprised loading, peak hold and unloading segments. Except for the peak hold segment, which was load controlled, all other segments were in displacement-controlled mode [35]. Loading and unloading segments were performed in constant indentation strain rate of 0.6 $s^{-1}$. In pyramidal indentation, constant indentation strain rate is achieved by maintaining the ratio of instant indentation speed to the instantaneous depth constant [35]. Indentation depth was set to 1.2 μm after contact load of 0.5 mN, which rests in total indentation depths of 1.4 μm. After attaining peak displacement during loading segment, the load was held constant for 3 s to allow the material to creep at peak hold segment. This was followed by constant strain rate unloading from the sample surface. At least 10 indents were performed on each Bulk sample and 3 indents were performed on each microdroplet. The whole loading/unloading cycles were done in less than 30 s. The indentation sites were selected from the thickest parts of the microdroplet to avoid any elastic influence from the fibre and to have the indenter tip oriented as close to the normal of the droplet surface as possible. The load–displacement data from each indentation was analysed with the Oliver-Pharr method [36] to estimate resin modulus and hardness and a minimum of three indents was done to each droplet to ensure consistency. The imaging during indentation used a LaB6 filament with 3.0 kV accelerating voltage. The accelerating voltage was kept low to avoid charging or other interaction with the sample.

## 3. Computational methods

The molecular network of the DGEBA epoxy and PEA hardener (see Fig. 1) system was modelled in the Maestro graphical interface of the Schrödinger Materials Suite (version 2023-1). The molecular dynamics (MD) calculations used established workflows with the Desmond/GPU code, capable of utilising the high level of parallelisation offered by modern graphical processing units (GPUs) [37]. The current version of the OPLS4 force-field [38–41] was used in all simulations. The overall simulation work comprised the following steps (number of simulation boxes after the simulation steps given in parentheses): Disordered system builder for creating the initial simulation boxes (5), Relaxation to equilibrate the simulation boxes (5), Crosslink polymers simulations to create crosslinked networks with various degrees of conversion (25), stress–strain simulations of the crosslinked networks (25).

To match the epoxy and amine hydrogen equivalent weights provided by the material manufacturers technical data sheets, a mixture of two structures for both epoxy and amine component was selected. The simulations began from the creation of five parallel simulation boxes with the Disordered system builder, through random snapped to grid placement molecules near the centre of the simulation box (steric packing) with van der Waals radii scaling factor of 0.5 to avoid overlaps. After placing the atoms, the simulation box was finalised with 3D orthorhombic periodic boundary conditions. The input molecules and the specific amount of each molecular structure input into the simulation boxes are presented in Table 1.

**Table 1**
Molecules used to create the simulation boxes for the epoxy resin simulations, the value n signifies repeating unit count. For the chemical structures of the components, refer to Fig. 1. The equivalent weight column refers to the epoxy equivalent weight and amine hydrogen equivalent weights of the mixture of different molecular weight components with the datasheet reference value in parentheses [32,33].

| Component | MW [g/mol] | Input molecules | Eq. weight [g/mol] |
|---|---|---|---|
| DGEBA, n=0 | 340.4 | 112 | 187.8 (185–192) |
| DGEBA, n=1 | 624.8 | 16 | |
| PEA, n=2 | 190.3 | 14 | 59.1 (60) |
| PEA, n=3 | 248.4 | 50 | |

The simulation boxes were relaxed through a multistep relaxation workflow comprising a total of 8 simulations described in detail in supplementary data S1. All simulations used the Nose–Hoover chain thermostat with a relaxation time of 1 ps and the NPT ensembles utilised the Martyna-Tobias-Klein barostat with isotropic coupling and a relaxation time of 2 ps. The dimensions of the simulation boxes, along with the equilibrated densities of the relaxed simulation boxes, are presented in supplementary data S1.

To create crosslinked networks, the simulation boxes were input to a Crosslink Polymers workflow. This Desmond/GPU workflow is a phenomenological, qualitative model that, instead of attempting to simulate real curing kinetics, forms crosslinks based on the following input criteria: maximum number of crosslinks per iteration, reaction threshold distance and the temperature dependent relative probabilities of the defined reactions. The reaction thresholds were cut-off distances in Ångstroms outside of which a complementary reactive site does not qualify for the reaction, set to 7 Å. The reaction probabilities were computed by the software based on primary and secondary amine reaction activation energies similarly to normalised Bolzmann factors, with the assumption there were no other energy states in the system than the reactions defined in the simulation input.

After forming a set of crosslinks based on the aforementioned criteria, the simulation boxes were equilibrated with MD for 50 ns NPT ensemble at 1.01325 bar. The thermostat target temperature is dependent on the iteration. All simulations (except $T_{max}$ = 300 K) included a simulated heating cycle of increasing temperature by 6.25 K per iteration up to $T_{max}$ followed by decreasing temperature by 6.25 K per iteration until it reaches 300 K or the simulation ends. This change in temperature affects both the probabilities of the defined reactions and the thermostat target temperature for the MD simulation. $T_{max}$

values were selected as 300 K, 400 K, 500 K, 600 K and 700 K to a total of five different average degrees of conversion with 5 parallel simulation boxes for each. These iterations were continued until one of the following conditions was met: the desired degree of conversion is reached or 20 consecutive iterations fail to form crosslinks — because no structures in the simulation box fulfil the defined criteria. The target conversion was set as 100% epoxide functionality, effectively causing the 20 iterations to be the only relevant end criterion. All temperature ramps were simulated starting from 300 K with the same "heating rate", up to a maximum temperature and back to 300 K, to create simulation boxes with different degrees of conversion by varying the maximum temperature. If the temperature ramp ended before the simulation end-criteria were met the iterations continued at 298.15 K. The primary purpose of the workflow was the creation of reasonably representative crosslinked structures for inputs to the stress–strain calculations. It was, however, also expected to provide some qualitative insight into the molecular mobility dependent kinetics at later stages of the crosslinking process.

The stress–strain calculation, in turn, incrementally deformed the simulation box and used Desmond/GPU to examine the system response to this strain from 1.5 ns NVT ensemble at 300 K simulations and recorded the pressure tensor at 5 ps intervals. Trajectory recording interval was set at 10 ps and stress was calculated from the last 20% of the trajectory. Strain rate was determined from the strain step size ($\Delta\varepsilon_1 = -0.0015$) and simulation time (1.5 ns) resulting in a strain rate of $10^6$ $s^{-1}$. Strain type was set as increased dilatation ($\eta = 0.33$). Further description on how these strain steps translate to simulation box deformations, and to the effective strain (and stress) reported in the results, are presented in supplementary data S1. To examine the effect of strain rate on the simulation result, the simulation for the $T_{max}$ = 600 K crosslinked networks was repeated with a strain rate of $10^7$ $s^{-1}$ – achieved by reducing the simulation time of the NVT ensemble to 150 ps.

No changes in chemical bonding were allowed in the stress–strain simulations, due to the non-reactive nature of the OPLS4 force-field. Covalent bonds were instead stretched according to their force-field determined potential until the simulation ends. This can cause erroneous results as eventually the energy needed to stretch a bond becomes extremely high. To mitigate this issue, compression was used as the primary mode of deformation and the maximum strain was kept low (<20%). Cyclic stress–strain simulation mode was enabled to provide results similar to the nanoindentation tests. The overall strain profile was set as 120 steps of compression followed by a single unloading/loading cycle with 80 simulation steps each. Results such as modulus and residual strain were analysed from the unloading cycle for consistency with the nanoindentation results.

## 4. Results and discussion

Volatile evaporation is the most commonly cited explanation to the difference in final conversion between samples of different length-scales. To study the phenomenon, a cooled resin mixture was inserted into a TGA coupled to an FTIR to analyse the chemical composition of any gasses evaporating during a controlled heating cycle. The results are presented in Fig. 2.

It is clear from the results that evaporation starts at relatively mild temperatures and based on the vibrations in the IR spectrum the volatile component evaporating is, as expected, the PEA hardener. From a sample inserted into the TGA, with volume in microlitres and open surface area around one millimeter squared, the evaporation is quite low as indicated by the low absorbance values, but detectable even from a larger sample batch such as this. A microdroplet has significantly higher relative surface area and the associated increase in vapour pressure likely both lowers the $T_{onset}$ and increases the intensity of the evaporation. As the heating of the sample is carried out until 350 °C the thermal degradation of the sample contributes to the detected gasses. However, the $CO_2$ associated vibrations around 2400 $cm^{-1}$ can be used to estimate when this degradation starts and these vibrations are detected to any significant degree only after a temperature of over 200 °C – well after the onset of the vibrations associated with the evaporation. Therefore, the TGA-FTIR measurement conclusively proves the role of hardener evaporation to the curing of the resin, at least for this epoxy — hardener combination. To support this result, the TGA-FTIR measurements were performed for samples comprising only one of the resin components at a time. These results are presented in supplementary data S2.

**Table 2**
Overview of DSC measurements of the epoxy resin system at different degrees of conversion. Measured from samples corresponding to those used in nanoindentation.

| Sample | Enthalpy [J/g] | $T_g$ [°C] | Degree of cure [%] |
|---|---|---|---|
| Bulk RT | 42.64 | 57.1 | 91.8 |
| Bulk 50 | 35.3 | 61.9 | 93.2 |
| Bulk RT-50 | 13.3 | 53.6 | 97.4 |
| Bulk 80 | 3.54 | 83.5 | 99.3 |
| Bulk RT-80 | 1.56 | 82.6 | 99.7 |

Dynamic DSC heating runs were used to study the conversion of the physical samples used as a point of comparison for the MD. Conversion analysed via DSC is discussed as degree of cure to differentiate it from the stoichiometric conversion discussed with the simulations. The degree of cure is determined based on the residual curing enthalpy compared to the total reaction enthalpy of the uncured resin. Pieces of the same bulk samples used for nanoindentation were subjected to two dynamic DSC heating steps to estimate the conversion. Care was taken, similarly to the nanoindentation samples, to measure an internal portion of the cured volume — both to strengthen the correlation with the nanoindentation and to minimise the contributions of evaporation. The conversion was analysed through comparison with the total reaction exotherm of a uncured resin sample, which was using the same DSC parameters determined as 520.6 J/g. After two heating cycles all samples exhibited a similar ultimate $T_g$ of 86.1 ± 1.9 °C. The results of the DSC analysis of the Bulk samples are presented in Table 2.

Nanoindentation was utilised to characterise the mechanical properties of microdroplets directly. The results from microdroplets were compared to the larger Bulk samples prepared from the same mixing batches. The modulus and hardness values along with analysed elastic and plastic energies from the indentation are presented in Table 3. Examples of SEM images and analysis plots are presented in supplementary data S3. The results immediately highlight the quite significant difference between the Bulk and droplet samples. Unfortunately, no direct comparison between the modulus and harness values of two sample types was found based on the results. Some of the common trends can still offer qualitative insights into the behaviour of the epoxy resin at different length-scales. Higher modulus values at lower degree of cure have been previously reported [31] and shown to be especially prominent as a sample surface phenomenon (shallow indentation depth). Similar results are shown here but cannot be – at least fully – attributed to surface effects. The Bulk samples were indented on a polished cross-sectional surface – mitigating the effects of evaporation – with a total indentation depth of over 1 μm as described earlier. Such effects could, however, contribute to the droplet results and the all-round higher measured modulus and hardness values they exhibit as the droplets are indented on their exposed surface.

The samples in Table 3 include two separate batches of samples, the first – done more as proof of concept – included 3 droplet samples and 1 large bulk resin sample cured 8 h at 80 °C. The samples were prepared identically in each case, except for the fact that the "Bulk ref" sample was not indented from a cut cross section but rather the closed mould surface. This might explain why the sample behaviour differs form all others especially in terms of the relative plastic/elastic indentation energies. The main difference of the two sample batches

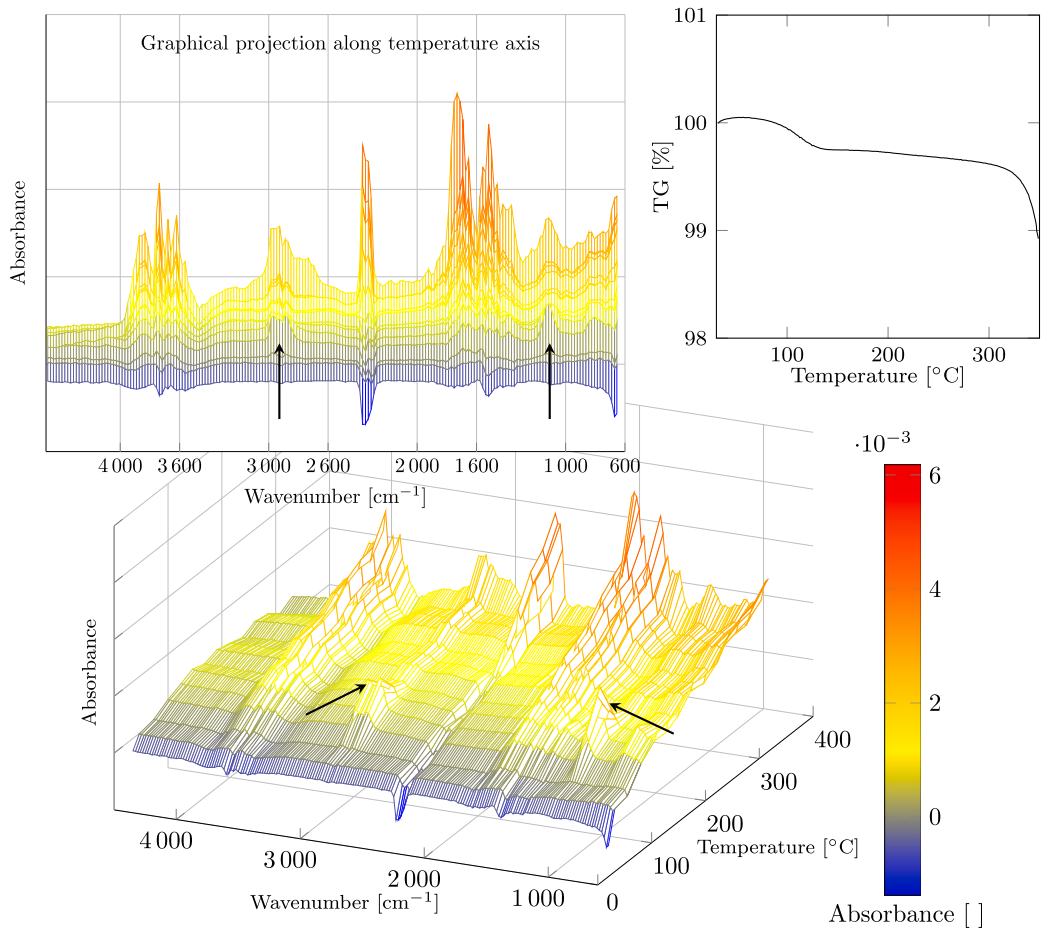


**Fig. 2.** FTIR coupled TGA measurement of the uncured resin mixture. The corresponding TGA result shown for reference. Arrows in the Figure indicate FTIR signals of evaporating hardener starting at $T_{onset} \approx 85$ °C.

**Table 3**
Overview of the nanoindentation results from different samples. Results represent the average of three indentations per sample.

| Sample | Hardness [MPa] | Modulus [GPa] | Hard./Mod. [MPa/MPa] | Plastic [%] | Elastic [%] |
|---|---|---|---|---|---|
| Droplet 1[a] | 302.8 ± 13.3 | 5.23 ± 0.12 | 0.058 ± 0.002 | 84.99 | 15.01 |
| Droplet 2[a] | 343.5 ± 20.6 | 5.47 ± 0.15 | 0.063 ± 0.002 | 84.20 | 15.80 |
| Droplet 3[a] | 235.0 ± 8.6 | 4.92 ± 0.33 | 0.048 ± 0.003 | 87.74 | 12.26 |
| Droplet 4 | 391.1 ± 20.5 | 5.30 ± 0.12 | 0.069 ± 0.003 | 87.12 | 12.88 |
| Droplet 5 | 361.4 ± 7.1 | 4.92 ± 0.09 | 0.074 ± 0.001 | 85.94 | 14.06 |
| Droplet 6 | 365.4 ± 11.2 | 5.15 ± 0.24 | 0.069 ± 0.004 | 86.63 | 13.37 |
| Droplet 7 | 351.9 ± 21.0 | 5.12 ± 0.14 | 0.074 ± 0.003 | 86.66 | 13.34 |
| Droplet 8 | 347.7 ± 3.6 | 4.70 ± 0.04 | 0.073 ± 0.003 | 86.28 | 13.72 |
| Droplet 9 | 346.1 ± 17.5 | 5.00 ± 0.10 | 0.071 ± 0.003 | 86.86 | 13.14 |
| Bulk ref[a] | 281.1 ± 8.3 | 4.19 ± 0.08 | 0.067 ± 0.003 | 79.52 | 20.48 |
| Bulk RT | 279.1 ± 7.1 | 4.37 ± 0.12 | 0.064 ± 0.002 | 85.44 | 14.56 |
| Bulk 50 | 271.8 ± 15.6 | 4.36 ± 0.20 | 0.062 ± 0.002 | 85.74 | 14.26 |
| Bulk RT-50 | 274.0 ± 4.8 | 4.40 ± 0.09 | 0.063 ± 0.002 | 84.55 | 15.45 |
| Bulk 80 | 272.5 ± 7.4 | 3.95 ± 0.07 | 0.069 ± 0.003 | 83.19 | 16.81 |

[a]Earlier batch of samples.

is, however, the time-frame of the measurement. Bulk ref and droplets 1–3 were tested within a month of mixing the resin and creation of the samples. For the rest there was an approximately 6 month wait from mixing and curing the resin to the actual testing. This explains especially the high mechanical performance of the Bulk RT sample, that has had plenty of time to post-cure during the 5–6 month window.

The best match between the macroscale Bulk samples and Droplets 4–9 was found based on the hardness/modulus ratio [31], which is consistently high for all droplets (average value 0.071 ± 0.004 MPa/MPa). The Bulk 80 sample, exhibits the similar – if slightly lower – ratio of 0.069 ± 0.003. The Bulk RT, Bulk 50 and Bulk RT-50 samples have average ratio of 0.063 ± 0.002. Therefore, the droplets should have an approximate degree of cure ⩾95% even considering evaporation and surface related effects. However, the hardness/modulus ratio of the earlier batch of droplets (Droplets 1–3) was significantly lower, only 0.056 ± 0.006, while for the Bulk ref sample the ratio was only slightly lower than the correspondingly cured Bulk 80 sample (0.067 ± 0.003). This would indicate that the degree of cure of the freshly prepared droplets was much lower, likely ⩽90%, and that post-curing and storage affect the droplets significantly, which is unsurprising but warrants further investigation. The testing of such samples should be at least timed consistently with the sample preparation.

MD simulations were used to study the effect of conversion of the resin system to its properties. In terms of conversion, the gel-point represents the biggest single change in properties. Another closely related term is known as vitrification and while the two are related the distinction is based on the observable change in behaviour. Gel point signifies the formation of an infinite polymer network and change from liquid-like to solid-like dominated behaviour. The classical theory for gel point determination is given by the Flory–Stockmayer theory [42,43], which gives the simulated systems described in Table 1 an estimated gel point of 56.4%. From the simulations, the gel point is determined either from the inflection point of the largest reduced molecular weight or from the maximum of the reduced molecular weight excluding the largest [25]. Both are proposed as representative points for the creation of a molecule percolating throughout the simulation box [25]. Examples these behaviours are presented in supplementary data S4 as

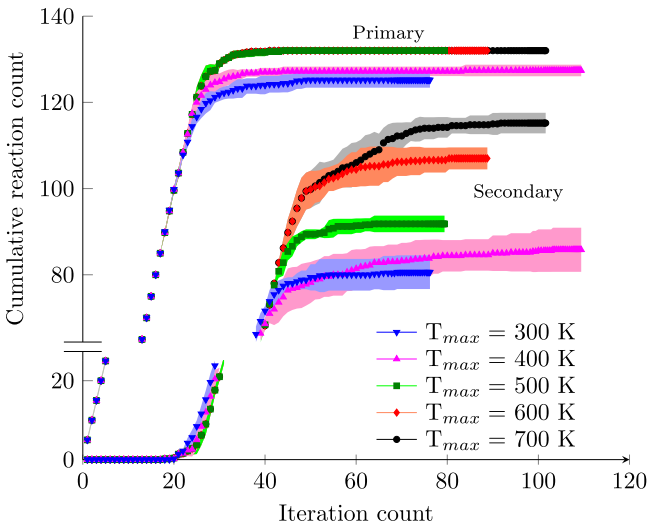


**Fig. 3.** Primary and secondary amine reactions during crosslinking simulations. Heating cycle simulations 300 K to $T_{max}$. The scatter plot represents the average and the shaded area the standard deviation of 5 parallel simulations.

first and second largest reduced molecular weight during the simulations. The two methods resulted in different values: the inflection point method resulted in a gel point of 61.6 ± 3.3% while the maximum method a somewhat higher value of 69.7 ± 4.1% conversion — possibly because only the second highest reduced molecular weight is considered instead of the weight-averaged reduced molecular weight. The gel point also represents the lowest conversion where the resin is expected to exhibit the properties of a solid or solid-like material. At lower conversions its physical nature is a high viscosity liquid and therefore conversions lower than the gel point are not worth of note in this context. Vitrification is more related to the onset of glass-like behaviour of the resin and is also temperature dependent (glass transition). Once vitrification occurs molecular mobility becomes almost impossible severely hindering further reactions unless the material is heated above the current glass transition temperature.

In addition to the gel point, monitoring the overall process of the conversion should help understand the formation of the polymer network and the final material properties. To visualise this, the numbers of primary and secondary amine reactions during the crosslinking simulation were monitored and the results are plotted in Fig. 3. In the early iterations in Fig. 3, the crosslinking simulation is representing the overall process poorly. At the early stages of curing the process is controlled by reaction energetics, which the simulation only considers in a probabilistic sense, meaning the early iterations were only limited by the maximum number of reactions allowed per iteration (5). After 16–20 iterations, slight differences between reaction conditions start to form. The cause is a combination of suitably high number of secondary amine moieties, the activation energy based probability criterion between the two amine types and the increasingly hindered molecular mobility due to already formed crosslinks. Gelling occurs around 30–40 iterations, considering the range of results for the gel point, after which molecular mobility becomes an important limitation to the formation of crosslinks and the simulation becomes significantly more realistic. This also coincides with the saturation of the primary amine reactions.

The crosslinking simulations presented above resulted in 25 different crosslinked systems, 5 for each $T_{max}$, which were treated as parallel samplings of a single average conversion. The crosslinked systems were input into the stress–strain simulations to estimate the mechanical properties vs. conversion behaviour. An example stress strain curve from $T_{max}$ = 700 K simulation box 3 is presented in Fig. 4. This stress strain simulation corresponded well with the average of the five parallel $T_{max}$ = 700 K simulation boxes. The modulus was estimated from the slope of the unloading curve – marked red in Fig. 4. Residual strain was likewise estimated form the unloading curve as the strain value at which stress is approximately equal to stress at zero strain. Residual strain was used mainly as a qualitative measure for comparison between identically deformed simulation boxes. Table 4 presents the primary outputs representing material performance for these different degrees of conversion.

**Table 4**
Overview of MD simulations of the epoxy resin system at different degrees of conversion. All values represent the average of 5 parallel simulations.

| $T_{max}$ [K] | Conversion [%] | Modulus [GPa] | Residual strain [%] |
|---|---|---|---|
| 300 | 81.7 ± 1.7 | 3.25 ± 0.84 | 10.6 ± 1.2 |
| 400 | 84.6 ± 2.4 | 3.90 ± 0.91 | 10.6 ± 0.8 |
| 500 | 88.8 ± 0.8 | 3.55 ± 1.12 | 9.6 ± 1.2 |
| 600 | 94.8 ± 1.1 | 3.44 ± 0.87 | 9.3 ± 0.8 |
| 700 | 98.1 ± 1.0 | 2.57 ± 1.19 | 9.4 ± 1.1 |

The simulations predicted similar trends as the nanoindentation: maximum conversion does not result in highest mechanical performance — or at least highest elastic modulus. Perfect agreement with experimental results was not expected as the result of such atomistic simulations is dependent not only on the strain rate and conversion, but also on system size, polymer chain length and entanglement and other similar factors. These last ones comprise the primary motivation for such simulations, allowing the observation of polymer morphology related contributions to observed properties. Based on the simulations, the modulus peaks at approximately 85% of the stoichiometric maximum conversion ($T_{max}$ = 400 K systems). This conversion also represented a significant outlier in the crosslinking simulations shown in Fig. 3. The variation of the results should also be considered an important factor. For example, the average modulus of $T_{max}$ = 700 K systems is only 2.57 GPa but for simulation box 1 the modulus is 4.5 GPa (stress–strain curve presented in supplementary data S4). Conversion is clearly not the most critical factor to the mechanical response of epoxy networks, at least above a certain threshold value.

As expected, strain rate affects these results somewhat. For the $T_{max}$ = 600 K systems repeating the simulations with a reduced MD stage time (150 ps) – increasing the strain rate to $10^{-7}$ $s^{-1}$ – reduced the average modulus to 3.16 ± 1.41 MPa and the residual strain to approximately 8.6 ± 1.2%. The average plots of the five parallel stress–strain simulations with the two strain rates are presented in supplementary data S5.

Interesting commonalities can also be found between the MD simulations and the nanoindentation results. In both cases, the most aggressive curing conditions – coinciding with the highest conversion – resulted in a lower elastic modulus compared to an 'optimal' curing cycle. Either result alone could be assumed as an erroneous or otherwise uncorrelated result. The MD simulations had very limited volume and likely cannot capture the full complexity of the epoxy morphology [15]. Conversely, the resin mixture placed into an 80 °C oven directly after casting will experience significant volatile evaporation from the open surface. The common trend, despite these differences, implies there is another phenomenon affecting the properties.

One reasonable hypothesis relates to molecular mobility – the gelling and vitrification of the resin – and the resulting morphology of the epoxy network. The maximum achievable conversion is determined by the possibility of the reactive reaching a suitable proximity and orientation. Not only does this always limit the conversion below 100%, but the molecular mobility throughout the curing reaction can change drastically between different curing conditions. For example consider two systems, one with slow conversion and sufficient time to relax internal stresses in the crosslinked network versus a system that reacts rapidly to a high conversion. These systems were exemplified in the atomistic simulations, by many of the $T_{max}$ = 400 K and 700 K

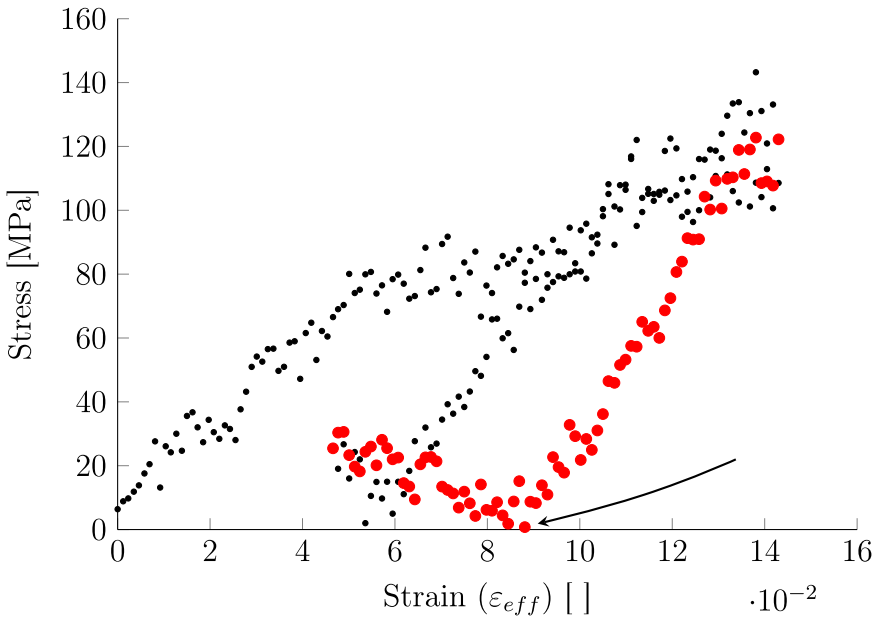


**Fig. 4.** Stress–strain simulation results for $T_{max}$ = 700 K simulation box 3. The unloading stage of the simulation is highlighted in red. Approximate residual strain is indicated with an arrow. Note that the data includes two loading stages. (For interpretation of the references to colour in this figure legend, the reader is referred to the web version of this article.)

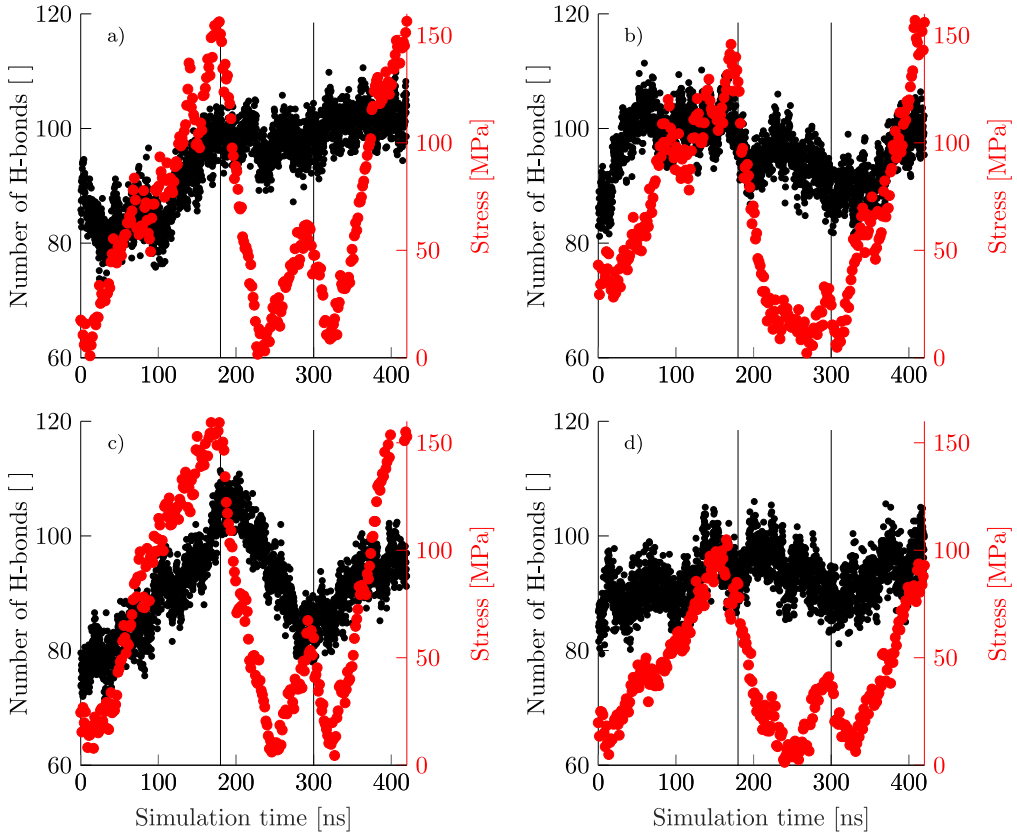


**Fig. 5.** Potential hydrogen bond interactions during the compressive stress–strain simulations of epoxy resin from selected simulation runs. Stresses are plotted in red for comparison. Vertical lines indicate different cyclic stress–strain stages. (a) $T_{max}$ = 400 K, (b) $T_{max}$ = 500 K, (c) $T_{max}$ = 600 K and (d) $T_{max}$ = 700 K. (For interpretation of the references to colour in this figure legend, the reader is referred to the web version of this article.)

crosslinked networks, respectively, as highlighted by the molecular weight development plots in supplementary data S4.

Additional hints were found based on the hydrogen bonding interactions during the trajectory of the stress–strain simulation. Stress curves representative of the specific conversions from $T_{max}$ = 500–700 K were selected and the estimated amount of hydrogen bonds during the trajectory are plotted in Fig. 5. The hydrogen bonds were estimated based on the criteria: maximum distance 2.8 Å, Donor minimum angle 120°, Acceptor minimum angle 90°. Aromatic hydrogen bonds are included but the software only considers the aromatic ring as a possible donor. To reduce the scatter in the hydrogen bond estimations a moving average on 5 was used to smooth the data for plotting. For many of

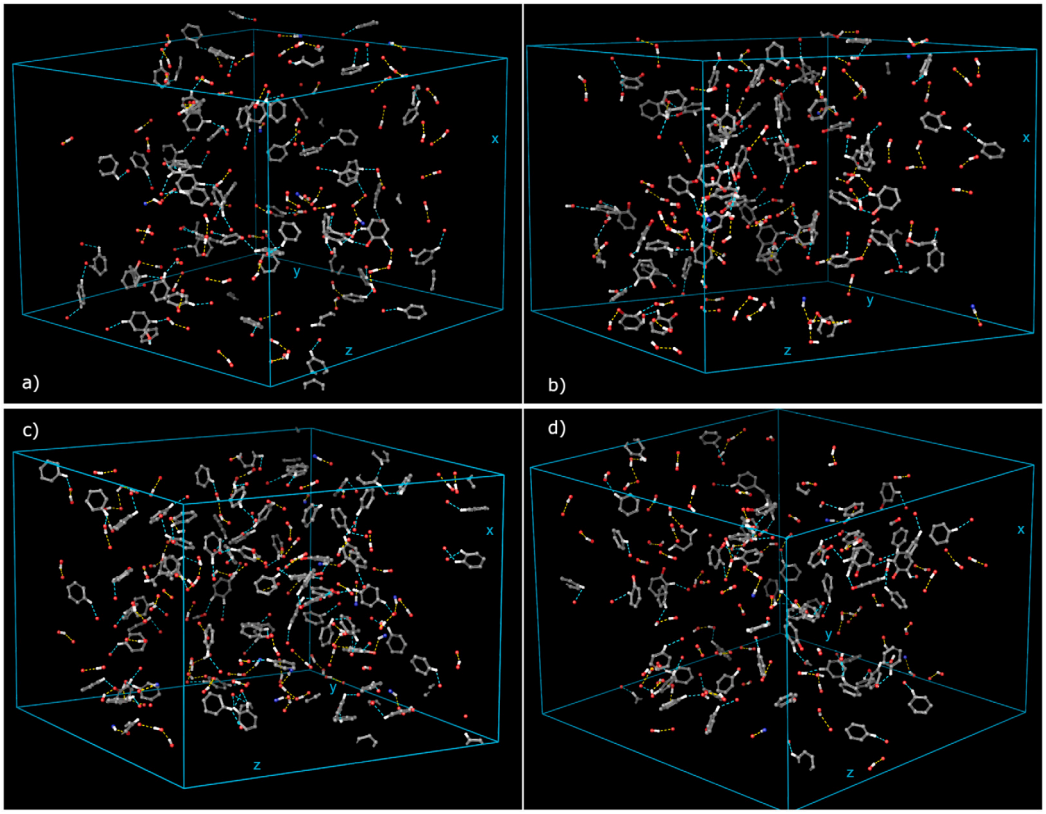


**Fig. 6.** Visualisation of functional groups participating in hydrogen bonding in the epoxy network during the $T_{max}$ = 600 K simulation box 2 stress–strain simulation. Black areas indicate areas with no H-bonding, not voids (atoms hidden from visualisation). The stress and hydrogen bond counts for this simulation are plotted in Fig. 5(c). Each pane represents a trajectory frame form the simulation: (a) frame 1 (0 ns), (b) frame 10478 (105 ns), (c) frame 18116 (181 ns) and (d) frame 24901 (249 ns).

the simulations, changes in the stress strain behaviour correlate with the predicted hydrogen bonding. Some simulations, however, show less changes in hydrogen bonding – such as Fig. 5(d) – and often also exhibit much lower stress levels during the deformation. While strain is not presented in Fig. 5, the strain in the simulation correlated linearly with simulation time. Unloading started after 180 ns and the second loading cycle after 300 ns.

To explore how this relates to the morphology of the polymer, a selected simulation box (corresponding to Fig. 5(c)) was carefully inspected visually. Four trajectory frames were selected from a single $T_{max}$ = 600 K simulation: the start of the simulation (Frame 1), first notable peak in hydrogen bonding at around 105 ns (Frame 10478), peak load at around 181 ns (Frame 18116) and the minimum load during unloading stage (Frame 24901). These are presented in Fig. 6.

The visualisation reveals specific regions of complex hydrogen bonded networks previously speculated also contributing to the curing kinetics [44]. These complex networks become more prominent with increasing strain and based on the hydrogen bonding — stress comparisons in Fig. 5 contribute to the mechanical response quite significantly. Many of the hydrogen bonds are formed either by aromatic hydrogens or the hydroxyl groups created by the epoxide-amine crosslinking reactions. Both areas of significant hydrogen bonding networks and areas completely without hydrogen bonding can be identified. Further work is needed to verify the result, as it is possible the observed local variations are a system size related anomaly. Nevertheless, considering also the role of the hydrogen bonds with varying conversion indicated in Fig. 5, this could also hint at changes in the epoxy morphology and the role of hydrogen bonding in the overall crosslinked network performance. As the highest stress–strain performance, high hydrogen bond counts and steadily progressing crosslinking simulations all coincide, it is could be that the ‘slower’ curing enables the epoxy network to orient favourably to maximise the hydrogen bonding contribution to the mechanical performance, whereas a rapidly vitrified network has no such advantage.

## 5. Conclusions

The curing of DGEBA based epoxy (EPON 828) with low molecular weight polyether amine hardener (Jeffamine D-230) in microcomposite samples was studied with a multiscale approach combining nanoindentation of macro- and microscale samples, thermal analysis and atomistic simulation. The results indicate the degree of cure of the resin the microdroplets was significantly lower than for similarly cured resin, but changes significantly with post-curing over time.

The evaporation of curing agent previously suggested as the cause of the discrepancy in the curing is shown through coupled TGA-FTIR measurement and offers at least a partial explanation. Based on the nanoindentation of samples with different curing cycles – supported by molecular dynamics simulations – the effect of different these curing cycles on the final properties is far from straightforward. This is likely a result of significant differences in the morphology of the epoxy network, which also contributes to the length-scale difference. Based on the stress–strain simulations, a significant portion of the difference can be attributed to differences in hydrogen bonding, which can stabilise the polymer networks with lower conversion leading to more homogeneous, or even improved, mechanical response compared to a rapidly vitrified, high degree of cure polymer network.

The original intent of this study was to find a pathway to evaluate – and hopefully correlate – the microdroplet specimen properties with those of macroscopic samples with similar conversion. However, these results indicate the length-scale discrepancy is unresolvable: the properties of a resin in microcomposite sample will never fully match those of a macroscopic sample, but careful and consistent sample preparation can somewhat mitigate the issue. The results also hint at much more

important concepts. Are the resin properties at different environments, in general, comparable? Is there a difference in the morphology of the resin in a composite compared to unreinforced resin? Answering these questions is crucial not only for improving the microcomposite interfacial tests but also to overall understanding of thermoset resin composites and remain a topic for future study.

## CRediT authorship contribution statement

**P. Laurikainen:** Conceptualization, Methodology, Formal analysis, Investigation, Data curation, Writing – original draft, Writing – review & editing, Visualization. **S. Bhusare:** Conceptualization, Formal analysis, Investigation, Writing – review & editing. **G. Mohanty:** Conceptualization, Methodology, Writing – review & editing, Supervision. **E. Sarlin:** Conceptualization, Resources, Writing – review & editing, Supervision.

## Declaration of competing interest

The authors declare that they have no known competing financial interests or personal relationships that could have appeared to influence the work reported in this paper.

## Data availability

Data will be made available on request.

## Acknowledgements

The study was financially supported by Jenny and Antti Wihuri foundation, Finland (Grant No. 00210182) and the Academy of Finland postdoctoral project: From micro-scale data to macro-scale understanding for improved safety of composite materials - MicMac (Grant No. 314983). S. Bhusare and G. Mohanty acknowledge partial use of funding from Academy of Finland grant 340192 for this work.

## Appendix A. Supplementary data

Supplementary material related to this article can be found online at https://doi.org/10.1016/j.polymer.2023.126148.

## References

[1] B. Miller, P. Muri, L. Rebenfeld, A microbond method for determination of the shear strength of a fiber/resin interface, Compos. Sci. Technol. 28 (1) (1987) 17–32, http://dx.doi.org/10.1016/0266-3538(87)90059-5.

[2] S. Zhandarov, E. Mäder, Peak force as function of the embedded length in pull-out and microbond tests: effect of specimen geometry, J. Adhes. Sci. Technol. 19 (10) (2005) 817–855, http://dx.doi.org/10.1163/1568561054929937.

[3] P. Laurikainen, M. Kakkonen, M. von Essen, O. Tanhuanpää, P. Kallio, E. Sarlin, Identification and compensation of error sources in the microbond test utilising a reliable high-throughput device, Composites A 137 (2020) 105988, http://dx.doi.org/10.1016/j.compositesa.2020.105988.

[4] E. Laukmanis, M. Janowski, S. Horn, J. Moosburger-Will, Effect of the interplay between fiber surface chemistry and sizing reactivity on fiber matrix interaction in carbon fiber reinforced epoxy resin, Compos. Interfaces (2022) 1–31, http://dx.doi.org/10.1080/09276440.2022.2068249.

[5] V. Rao, L.T. Drzal, Loss of curing agent during thin film (droplet) curing of thermoset material, J. Adhes. 35 (4) (1991) 245–249, http://dx.doi.org/10.1080/00218469108041011.

[6] D. Bryce, J. Thomason, L. Yang, Micromechanical and spectroscopic characterisation of the curing performance of epoxy resins in the microbond test, IOP Conf. Ser.: Mater. Sci. Eng. 942 (1) (2020) 012019, http://dx.doi.org/10.1088/1757-899x/942/1/012019.

[7] P. Zinck, H. Wagner, L. Salmon, J. Gerard, Are microcomposites realistic models of the fibre/matrix interface? Ii. physico-chemical approach, Polymer 42 (15) (2001) 6641–6650, http://dx.doi.org/10.1016/S0032-3861(00)00871-5.

[8] N. Rahmani, B. Willard, K. Lease, E.T. Legesse, S.A. Soltani, S. Keshavanarayana, The effect of post cure temperature on fiber/matrix adhesion of T650/cycom 5320-1 using the micro-droplet technique, Polym. Test. 46 (2015) 14–20, http://dx.doi.org/10.1016/j.polymertesting.2015.05.012.

[9] F. Meyer, G. Sanz, A. Eceiza, I. Mondragon, J. Mijović, The effect of stoichiometry and thermal history during cure on structure and properties of epoxy networks, Polymer 36 (7) (1995) 1407–1414, http://dx.doi.org/10.1016/0032-3861(95)95918-Q.

[10] R.F. Minty, L. Yang, J.L. Thomason, The influence of hardener-to-epoxy ratio on the interfacial strength in glass fibre reinforced epoxy composites, Composites A 112 (2018) 64–70, http://dx.doi.org/10.1016/j.compositesa.2018.05.033.

[11] H. Li, G. Chen, H. Su, D. Li, L. Sun, J. Yang, Effect of the stoichiometric ratio on the crosslinked network structure and cryogenic properties of epoxy resins cured at low temperature, Eur. Polym. J. 112 (2019) 792–798, http://dx.doi.org/10.1016/j.eurpolymj.2018.10.051.

[12] R. Unger, U. Braun, J. Fankhänel, B. Daum, B. Arash, R. Rolfes, Molecular modelling of epoxy resin crosslinking experimentally validated by near-infrared spectroscopy, Comput. Mater. Sci. 161 (2019) 223–235, http://dx.doi.org/10.1016/j.commatsci.2019.01.054.

[13] J. Thomason, An overview of some scaling issues in the sample preparation and data interpretation of the microbond test for fibre-matrix interface characterisation, Polym. Test. 111 (2022) 107591, http://dx.doi.org/10.1016/j.polymertesting.2022.107591.

[14] P. Laurikainen, S. Pötz, J. Jokinen, M. von Essen, M. Lindgren, P. Kallio, M. Kanerva, G. Oreski, E. Sarlin, High-throughput mechanical micro-scale characterization of composites and the utilization of the results in finite element analysis, in: Proceedings of the 18th European Conference on Composite Materials, European Society of Composite Materials, 2018.

[15] C.M. Sahagun, K.M. Knauer, S.E. Morgan, Molecular network development and evolution of nanoscale morphology in an epoxy-amine thermoset polymer, J. Appl. Polym. Sci. 126 (4) (2012) 1394–1405, http://dx.doi.org/10.1002/app.36763.

[16] S. Morsch, Y. Liu, P. Greensmith, S.B. Lyon, S.R. Gibbon, Molecularly controlled epoxy network nanostructures, Polymer 108 (2017) 146–153, http://dx.doi.org/10.1016/j.polymer.2016.11.050.

[17] P.V. Komarov, C. Yu-Tsung, C. Shih-Ming, P.G. Khalatur, P. Reineker, Highly cross-linked epoxy resins: An atomistic molecular dynamics simulation combined with a mapping/reverse mapping procedure, Macromolecules 40 (22) (2007) 8104–8113, http://dx.doi.org/10.1021/ma070702+.

[18] Z. Meng, M.A. Bessa, W. Xia, W. Kam Liu, S. Keten, Predicting the macroscopic fracture energy of epoxy resins from atomistic molecular simulations, Macromolecules 49 (2016) 9474–9483, http://dx.doi.org/10.1021/acs.macromol.6b01508.

[19] T. Hobbiebrunken, B. Fiedler, M. Hojo, M. Tanaka, Experimental determination of the true epoxy resin strength using micro-scaled specimens, Composites A 38 (3) (2007) 814–818, http://dx.doi.org/10.1016/j.compositesa.2006.08.006.

[20] N.J. Soni, P.-H. Lin, R. Khare, Effect of cross-linker length on the thermal and volumetric properties of cross-linked epoxy networks: A molecular simulation study, Polymer 53 (4) (2012) 1015–1019, http://dx.doi.org/10.1016/j.polymer.2011.12.051.

[21] C.E. Estridge, The effects of competitive primary and secondary amine reactivity on the structural evolution and properties of an epoxy thermoset resin during cure: A molecular dynamics study, Polymer 141 (2018) 12–20, http://dx.doi.org/10.1016/j.polymer.2018.02.062.

[22] M. Blanco, M.A. Corcuera, C.C. Riccardi, I. Mondragon, Mechanistic kinetic model of an epoxy resin cured with a mixture of amines of different functionalities, Polymer 46 (19) (2005) 7989–8000, http://dx.doi.org/10.1016/j.polymer.2005.06.117, Controlled Macromolecular Synthesis and Controlled Architectures - Supramolecular Polymer Assemblies.

[23] R. Hardis, J.L. Jessop, F.E. Peters, M.R. Kessler, Cure kinetics characterization and monitoring of an epoxy resin using DSC, Raman spectroscopy, and DEA, Composites A 49 (2013) 100–108, http://dx.doi.org/10.1016/j.compositesa.2013.01.021.

[24] N. Sbirrazzuoli, S. Vyazovkin, A. Mititelu, C. Sladic, L. Vincent, A study of epoxy-amine cure kinetics by combining isoconversional analysis with temperature modulated DSC and dynamic rheometry, Macromol. Chem. Phys. 204 (15) (2003) 1815–1821, http://dx.doi.org/10.1002/macp.200350051.

[25] C. Li, A. Strachan, Molecular scale simulations on thermoset polymers: A review, J. Polym. Sci. B: Polym. Phys. 53 (2) (2015) 103–122, http://dx.doi.org/10.1002/polb.23489.

[26] L.J. Abbott, K.E. Hart, C.M. Colina, Polymatic: a generalized simulated polymerization algorithm for amorphous polymers, Theor. Chem. Acc. 132 (2013) http://dx.doi.org/10.1007/s00214-013-1334-z, 1334.

[27] G.M. Odegard, B.D. Jensen, S. Gowtham, J. Wu, J. He, Z. Zhang, Predicting mechanical response of crosslinked epoxy using reaxff, Chem. Phys. Lett. 591 (2014) 175–178, http://dx.doi.org/10.1016/j.cplett.2013.11.036.

[28] B. Damirchi, M. Radue, K. Kanhaiya, H. Heinz, G.M. Odegard, A.C.T. van Duin, Reaxff reactive force field study of polymerization of a polymer matrix in a carbon nanotube-composite system, J. Phys. Chem. C 124 (37) (2020) 20488–20497, http://dx.doi.org/10.1021/acs.jpcc.0c03509.

[29] G.M. Odegard, S.U. Patil, P.P. Deshpande, K. Kanhaiya, J.J. Winetrout, H. Heinz, S.P. Shah, M. Maiaru, Molecular dynamics modeling of epoxy resins using the reactive interface force field, Macromolecules 54 (21) (2021) 9815–9824, http://dx.doi.org/10.1021/acs.macromol.1c01813.

[30] C.D. Petruczok, R. Yang, K.K. Gleason, Controllable cross-linking of vapor-deposited polymer thin films and impact on material properties, Macromolecules 46 (5) (2013) 1832–1840, http://dx.doi.org/10.1021/ma302566r.
[31] S. Ligot, E. Bousser, D. Cossement, J. Klemberg-Sapieha, P. Viville, P. Dubois, R. Snyders, Correlation between mechanical properties and cross-linking degree of ethyl lactate plasma polymer films, Plasma Process. Polym. 12 (6) (2015) 508–518, http://dx.doi.org/10.1002/ppap.201400162.
[32] HEXION Specialty Chemicals, EPON Resin 828, 2005, Technical data sheet.
[33] Huntsman Corporation, JEFFAMINE d-230 polyetheramine, 2007, Technical data sheet.
[34] P. Laurikainen, R. Dsouza, M. Kakkonen, M. Kanerva, E. Sarlin, Exploring the role of fibre sizing to the fatigue of glass fibre composites using a novel, reliable micro-fatigue test, Composites A (2023) 107425, http://dx.doi.org/10.1016/j.compositesa.2023.107425.
[35] J. Wehrs, G. Mohanty, G. Guillonneau, A.A. Taylor, D. Maeder, L. Philippe, S. Mischler, J.M. Wheeler, J. Michler, Comparison of in situ micromechanical strain-rate sensitivity measurement techniques, JOM 67 (8) (2015) 1684–1693, http://dx.doi.org/10.1007/s11837-015-1447-z.
[36] W. Oliver, G. Pharr, Measurement of hardness and elastic modulus by instrumented indentation: Advances in understanding and refinements to methodology, J. Mater. Res. 19 (1) (2004) 3–20, http://dx.doi.org/10.1557/jmr.2004.19.1.3.
[37] M. Bergdorf, S. Baxter, C.A. Rendlman, D. Shaw, Desmond/GPU Performance as of November 2016, Technical Report, D. E. Shaw Research, 2016, URL https://www.deshawresearch.com/publications.
[38] OPLS4, Schrödinger, Inc., 2021.
[39] C. Lu, C. Wu, D. Ghoreishi, W. Chen, L. Wang, W. Damm, G.A. Ross, M.K. Dahlgren, E. Russell, C.D. Von Bargen, R. Abel, R.A. Friesner, E.D. Harder, OPLS4: Improving force field accuracy on challenging regimes of chemical space, J. Chem. Theory Comput. 17 (7) (2021) 4291–4300, http://dx.doi.org/10.1021/acs.jctc.1c00302, PMID: 34096718.
[40] K. Roos, C. Wu, W. Damm, M. Reboul, J.M. Stevenson, C. Lu, M.K. Dahlgren, S. Mondal, W. Chen, L. Wang, R. Abel, R.A. Friesner, E.D. Harder, OPLS3e: Extending force field coverage for drug-like small molecules, J. Chem. Theory Comput. 15 (3) (2019) 1863–1874, http://dx.doi.org/10.1021/acs.jctc.8b01026, PMID: 30768902.
[41] K.H. DuBay, M.L. Hall, T.F. Hughes, C. Wu, D.R. Reichman, R.A. Friesner, Accurate force field development for modeling conjugated polymers, J. Chem. Theory Comput. 8 (11) (2012) 4556–4569, http://dx.doi.org/10.1021/ct300175w, PMID: 26605615.
[42] P.J. Flory, Molecular size distribution in three dimensional polymers. i. Gelation1, J. Am. Chem. Soc. 63 (11) (1941) 3083–3090, http://dx.doi.org/10.1021/ja01856a061.
[43] W.H. Stockmayer, Theory of Molecular Size Distribution and Gel Formation in Branched Polymers II. General Cross Linking, J. Chem. Phys. 12 (4) (1944) 125–131, http://dx.doi.org/10.1063/1.1723922.
[44] P.V. Laurikainen, E.L. Sarlin, Cut-off scale and complex formation in density functional theory computations of epoxy-amine reactivity, ACS Omega 6 (44) (2021) 29424–29431, http://dx.doi.org/10.1021/acsomega.1c03229.